Elucidating Optimal Nanohole Structures for Suppressing Phonon Transport in Nanomeshes

Haoran Cui¹, Tengfei Ma²‡ and Yan Wang³§

Department of Mechanical Engineering, University of Nevada, Reno, Reno, NV 89557

5 May 2024

Abstract. Nanomeshes, often referred to as phononic crystals, have been extensively explored for their unique properties, including phonon coherence and ultralow thermal conductivity (κ). However, experimental demonstrations of phonon coherence are rare and indirect, often relying on comparison with numerical modeling. Notably, a significant aspect of phonon coherence, namely the disorder-induced reduction in κ observed in superlattices, has yet to be experimentally demonstrated. In this study, through atomistic modeling and spectral analysis, we systematically investigate and compare phonon transport behaviors in graphene nanomeshes, characterized by 1D line-like hole boundaries, and silicon nanomeshes, featuring 2D surface-like hole boundaries, while considering various forms of hole boundary roughness. Our findings highlight that to demonstrate a disorder-induced reduction in κ of nanomeshes, optimal conditions include low temperature, smooth and planar hole boundaries, and the utilization of thick films composed of 3D materials.

1. Introduction

Nanomeshes (NMs), also known as phononic crystals, are holey membranes made of materials such as graphene[1], silicon[2], and others. These structures have been extensively studied for their distinctive thermal transport properties, notably ultralow κ and phonon coherence[2–5], both arising from phonon-nanohole scattering in various forms.

The pursuit of ultralow thermal conductivity (κ) in NMs has been longstanding, driven by their potential applications in thermoelectrics[3, 6]. In NMs, incoherent phonons[7, 8], behaving predominantly like particles, encounter significant obstruction and scattering from the numerous nanoholes, contributing significantly to the observed ultralow κ . Furthermore, emerging evidence, supported by several experiments, affirms that coherent phonons, exhibiting more wave-like behavior, experience strong backscattering at nanoholes, resulting in the formation of substantial phonon band gaps[2, 5]. This phenomenon leads to a κ even lower than what is anticipated for the incoherent phonon case.

[‡] Co-first author with equal contribution

[§] E-mail address:yanwang@unr.edu

To date, superlattice (SL) and NM stand out as the two extensively studied nanostructures showcasing substantial phonon coherence. Notably, SLs have emerged as a more successful system[9–16], demonstrating various coherent phonon transport behaviors both experimentally and theoretically. A distinctive hallmark of phonon coherence is the substantial reduction of κ when disorder in layer thickness is introduced to an initially periodic SL[10, 14]. This disorder-induced reduction in κ has been consistently observed across various SL systems and is commonly attributed to the localization of coherent phonons.

The direct, unambiguous experimental demonstrations of phonon coherence in NM structures are much rarer compared to the success in SLs. Pioneering experiments have showcased the ultralow κ of silicon NMs[2, 4, 5], defying explanations solely based on incoherent phonon (i.e., phonon particle) theory. This anomalous behavior has been attributed to coherent phonon backscattering and bandgap formation. However, attempts for a more direct demonstration of phonon coherence in NMs have faced challenges. A notable study by Lee et al. [17] found no disorder-induced reduction in κ in silicon NMs, where samples with periodically arranged holes exhibited similar κ to those with aperiodically arranged holes across a wide temperature range from 14 K to 325 K. This lack of distinction does not necessarily negate the existence of phonon coherence in NMs; instead, it might be constrained by the quality of hole boundary surfaces. Research on SLs has established that roughness or other structural irregularities can impede phonon coherence [18–20]. While current fabrication techniques make it challenging to provide conclusive evidence, recent molecular dynamics studies have effectively demonstrated significant reductions in κ caused by disorders in hole locations in NMs composed of various materials, such as graphene and silicon[21, 22]. However, the quest for identifying the optimal NM systems (including hole designs, material choices, and ambient conditions) that allow experimentalists to observe disorder-induced reductions in κ remains elusive. This limitation hinders a comprehensive understanding of phonon coherence in NMs and the design of ultralow- κ NMs for thermoelectric applications.

Recognizing hole boundary surface roughness as a crucial factor limiting experiments on NMs, our work aims to delve into the impact of hole surface roughness on phonon coherence in NMs made of 2D and 3D materials. We will specifically focus on two types of structures: graphene nanomesh (GNM) and silicon nanomesh (SNM). In the 2D GNM, roughness manifests as 1D line roughness, while in the 3D SNM, roughness takes the form of 2D surface roughness. A meticulous comparison of these two systems is anticipated to illuminate the varying effects of roughness on phonon coherence in 2D and 3D materials. Furthermore, such a comparative analysis may provide valuable insights into identifying optimal material systems for more effectively demonstrating phonon coherence in experimental settings. GNMs and SNMs, both possessing potentially ultralow lattice κ , have been proposed as excellent thermoelectric materials [6, 23], benefiting from low κ to achieve high figure-of-merits. It is thus crucial to investigate optimal structural and material features to minimize the κ of nanomesh structures.

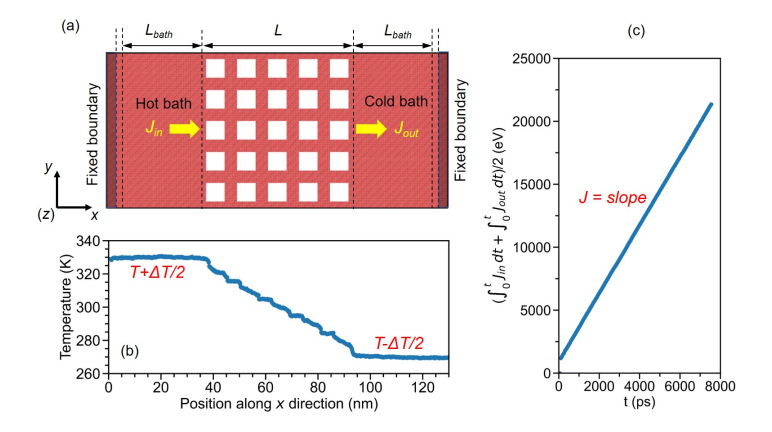


Figure 1: (a) Schematic of the simulation domain setup in NEMD simulation in LAMMPS. L_{bath} is the length of heat bath and L is the total length of the device. Hot and cold baths are maintained at $T + \Delta T/2$ and $T - \Delta T/2$, respectively. J represents the steady-state heat current. (b) Temperature profile along the x (heat flow) direction. (c) Cumulative energy flow between hot bath and cold bath as a function of time, of which the slope is heat current.

2. Methodology

2.1. Equilibrium molecular dynamics

The bulk-limit κ of GNM and SNM is calculated through equilibrium molecular dynamics (EMD) simulations using the Green-Kubo method. All simulations are executed employing the LAMMPS package[24]. Specifically, the interactions of silicon atoms are characterized using the Stillinger-Weber (SW) potential[25], while the Tersoff potential[26] is employed to describe C-C interactions in graphene. The simulation timestep is set as 0.5 fs, and periodic boundary conditions are applied to the entire structure in all three orientations to eliminate the influence of fixed walls.

In the simulation process, the temperature of the entire system is gradually raised from 5.0 K to the target temperatures (200 K, 300 K, 400 K) within the constant NPT ensemble for 1,000 ps (2 million time-steps) using a Nose-Hoover temperature thermostat and Nose-Hoover pressure barostat. To ensure the temperature of the whole system matches the target temperature, an additional constant NPT integration is performed to equilibrate the structure at target temperatures for 2,000 ps (4 million time-steps). Ultimately, the calculation of the heat flux vector is conducted for 7,500 ps (15 million time-steps) within the simulation under the NVE ensemble, from which κ is obtained using the Green-Kubo method.

2.2. Nonequilibrium molecular dynamics

The domain setup of non-equilibrium molecular dynamics (NEMD) simulations is shown in Fig. 1. The NM with length L (61 nm) is sandwiched between two heat baths with

length L_{bath} (34 nm). Roughly 0.7 nm thick of atoms (the dark regions) at the two ends of the model are frozen, which could be regarded as fixed boundary condition that fixes the structure in space and blocks heat transfer across the periodic boundary.

Similar to EMD simulations, we employ the SW potential[25] for SNM and the Tersoff potential[26] for GNM. The periodic boundary condition is applied to all three dimensions. Meanwhile, we assign a random velocity vector to each atom based on a Gaussian distribution with a mean initial temperature of 5 K, and the time-step is set at 0.5 fs. Subsequently, the NM structure is relaxed in the NPT ensemble at zero pressure. During this relaxation, we gradually increase the system temperature from 5 K to target temperatures (200 K, 300 K, or 400 K) over 1,000 ps.

To ensure the system is fully relaxed at the target temperature, the entire structure undergoes additional relaxation in an NPT ensemble at zero pressure and the target temperature for 2,000 ps. Following this, the NEMD simulation is conducted for 7,500 ps, during which the hot and cold baths are maintained at $T + \Delta T/2$ and $T - \Delta T/2$, respectively. Fig.1(b) illustrates a typical temperature profile obtained in our NEMD simulations, and Fig.1(c) displays the corresponding heat flow data. Finally, κ is calculated as

$$\kappa = \frac{J \cdot L}{\Delta T \cdot A_c},\tag{1}$$

where A_c is the cross-sectional area of the device, J is the steady-state heat current, L is the length of the device, and ΔT is the temperature difference between hot and heat baths.

2.3. Spectral phonon heat flux analysis

To elucidate the mechanisms governing thermal transport in the diverse simulated structures, we perform spectral phonon transmission analysis for the same set of our NEMD simulations. In particular, we calculate the spectrally decomposed heat flux in our NEMD simulations using Eq. 2 to quantify phonon transmission [27, 28]:

$$Q(\omega) = \sum_{i \in \tilde{L}} \sum_{j \in \tilde{R}} \left(-\frac{2}{t_{simu}\omega} \sum_{\alpha,\beta} Im \langle \hat{v}_i^{\alpha}(\omega)^* K_{ij}^{\alpha\beta} \hat{v}_j^{\beta}(\omega) \rangle \right), \tag{2}$$

in which $Q(\omega)$ is the spectral heat current, ω is the frequency, i and j are respectively the atom indices in the left(\tilde{L}) and right(\tilde{R}) part of a chosen cross section, t_{simu} is the total NEMD simulation time, α and β are Cartesian coordinates, \hat{v} is the Fourier transform of atom velocity, * denotes the complex conjugate, and $K_{ij}^{\alpha\beta}$ is the force constant matrix.

2.4. Model systems

In this study, we will investigate groups of NMs characterized by different nanohole geometries (circular or square), surface roughness (rough or smooth), and hole distributions (periodic or aperiodic), all possessing equivalent porosity.

To explore the influence of nanohole geometries on κ , we study NMs featuring both circular and square holes. These holes, positioned at identical locations, exhibit dimensions of approximately 7.3 nm \times 7.3 nm for square holes and a diameter of roughly 8.2 nm for circular ones, ensuring consistent porosity across the structures.

To elucidate the impact of surface roughness on κ , we study nanoholes with both smooth and rough surfaces. Surface roughness was quantified by calculating the root-mean-square deviation of atomic coordinates from ideal square or circular shapes corresponding to the holes. The resulting roughness values for square-smooth, square-rough, circular-smooth, and circular-rough SNMs are 0 \mathring{A} , 0.6318 \mathring{A} , 0.5039 \mathring{A} , and 0.9021 \mathring{A} , respectively. Similarly, for GNMs, the corresponding roughness values are 0 \mathring{A} , 0.5788 \mathring{A} , 0.4325 \mathring{A} , and 0.7136 \mathring{A} . Notably, GNMs generally exhibit lower roughness values compared to SNMs due to their single-layer atomic structure.

Additionally, we will investigate NMs with both periodic and aperiodic arrangements of holes to assess the influence of hole distribution on κ . Specifically, we will explore three distinct aperiodic NMs, and the average κ was calculated to account for variations in hole locations within these structures.

The influence of lattice orientation on the thermal, optical, and electrical properties of 2D materials, including graphene, is well established. This effect becomes particularly pronounced when graphene is engineered into nanostructures like graphene nanoribbons [29], carbon nanotubes (which can be conceptualized as rolled graphene) [30], and nanomeshes [21, 31]. In the case of GNMs, holes can exhibit different chiralities—zigzag or armchair—depending on their orientation relative to the graphene lattice, thereby impacting phonon transport to varying degrees. As discussed in Ref. [29], these distinct edge chiralities can induce different levels of boundary scattering or phonon localization, consequently influencing thermal transport. Additionally, the shape of holes in GNMs has been shown to exert a significant effect on thermal transport [21, 31]. Square holes, with two boundaries parallel to the heat flow direction, and circular holes represent two extremes in hole geometry. The former acts as a specular boundary to phonons, while the latter constitutes a more diffuse boundary, leading to reduced thermal conductivity. Therefore, in this study, we focus our investigations on these two prototypical hole shapes, ensuring generality in the conclusions drawn from our research.

As a final note, since molecular dynamics (MD) naturally simulates atomic motion and their interactions, any phonon interference process can be naturally captured, if present. Thus, MD has the unique advantage of modeling coherent phonon transport behaviors in materials. Recent studies have shown that MD can rigorously model the transmission, reflection, and interference of phonons [32, 33]. Therefore, our simulations can capture these effects effectively. However, it is important to note that classical MD simulations are based on Newton's laws of motion and cannot represent quantum effects present in classical systems. Quantum behaviors, which are missing in classical MD, include temperature-dependent phonon heat capacities and corresponding phonon lifetimes, as well as quantum tunneling and others. We assert that they may affect the modeling results quantitatively but do not alter the conclusions regarding the impact of

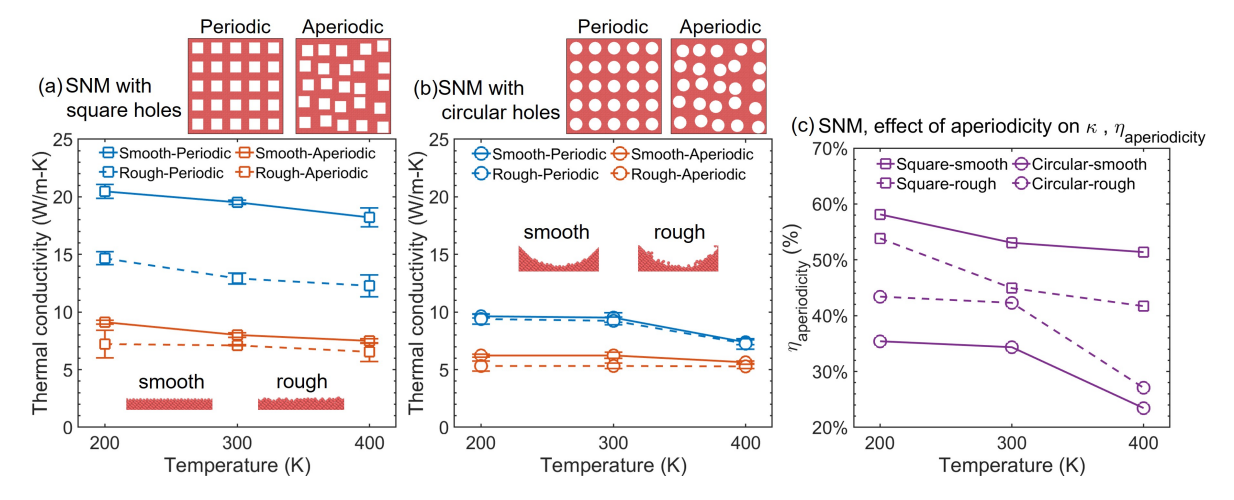


Figure 2: κ of SNMs at different temperatures. (a) SNMs with square holes. (b) SNMs with circular holes. (c) The effectiveness of aperiodicity in reducing κ .

different hole shapes or roughness on phonon coherence. For the above reason, classical MD has been a popular tool for investigating thermal transport in materials, including at low-temperature conditions, to reveal essential physics qualitatively.

3. Results and Discussions

3.1. Silicon Nanomesh

3.1.1. Effect of hole shape, boundary roughness, and distribution on κ Through EMD simulations, we obtain the κ of SNMs featuring either square or circular holes, arranged in periodic or aperiodic patterns, with respect to temperature, as illustrated in Figs. 2a and 2b. Notably, we can draw similar conclusions as previous studies regarding certain well-known behaviors of phonon thermal transport in NMs.

Firstly, in all cases, κ decreases with rising temperature. This agrees with previous experiments [17, 34] and molecular dynamics (MD) simulations [35] that have consistently demonstrated that κ decreases at higher temperatures, attributed to intensified anharmonic scattering. Nonetheless, the κ of NMs typically has a milder temperature dependence than that of pristine materials. This is a characteristic of materials with strong extrinsic scattering, such as hole-boundary scattering in NMs [21] and interface scattering in superlattices [20]. Additionally, we conduct harmonically-mapped averaging (HMA) analysis [36] and spectral phonon energy density (SED) analysis [37, 38] to assess how anharmonic effects change with temperature. It is important to note that both HMA and SED methods, integrated into MD, inherently incorporate any anharmonic effects within the material. As illustrated in Fig. S1 of the Supplementary Materials, the HMA analysis results, which quantify the degree of lattice anharmonicity at a specific temperature, reveal increased anharmonicity with temperature. Furthermore, depicted in Fig. S2 of the Supplementary Materials, the

SED analysis results, which quantify the degree of anharmonic phonon scattering, show a decrease in phonon lifetime at higher temperatures. Thus, both the rise in lattice anharmonicity and anharmonic phonon scattering contribute to the reduced κ of SNMs at higher temperatures.

Furthermore, SNMs with square holes exhibit higher κ compared to their counterparts with circular holes, because phonons are scattered more diffusely by circular holes than by square ones. Another less important mechanism lies in the slight difference in the width of phonon transport channels. Despite both configurations having equivalent porosity, the smaller side length of square holes in comparison to the diameter of circular holes results in wider channels in NMs with square holes. Notably, Yarifard et al.[31] emphasized the significance of channel width, or neck width, as a critical parameter influencing the κ of NMs.

Lastly, SNMs with periodically arranged holes demonstrate higher κ than those with aperiodically arranged holes, forming the central focus of our investigation. The diminished κ in aperiodic NMs can be attributed to two mechanisms. First, the randomly distributed holes disrupt the otherwise straight channels present in periodic NMs, significantly impeding phonon transport and resulting in reduced κ . Second, the disordered hole locations may localize phonons, as indicated by previous studies on the impact of secondary periodicity and aperiodicity on phonon transport. Notably, investigations into the lattice κ of aperiodic SLs have consistently shown substantially lower values compared to their periodic counterparts, a phenomenon supported by both experimental evidence and modeling.

3.1.2. The effectiveness of hole aperiodicity in reducing κ : contributing factors. A more substantial distinction between κ_{periodic} and $\kappa_{\text{aperiodic}}$ has been pursued, driven by the imperative of minimizing κ in specific applications, such as in thermoelectric materials. To comprehensively evaluate the effectiveness of hole distribution in reducing κ , we introduce a new parameter, $\eta_{\text{aperiodicity}}$, which quantifies the influence of aperiodic hole locations on the κ of NM structures. Specifically, $\eta_{\text{aperiodicity}}$ is defined as

$$\eta_{\text{aperiodicity}} = 1 - \frac{\kappa_{\text{aperiodic}}}{\kappa_{\text{periodic}}}.$$
(3)

As illustrated in Fig. 2c, with increasing temperature, the quantity $\eta_{\text{aperiodicity}}$ gradually diminishes, suggesting a diminishing advantage in randomizing hole locations. The apparent rationale behind this trend lies in the fact that the κ of periodic NMs decreases more rapidly with rising temperature compared to aperiodic NMs. This phenomenon indicates a weaker phonon coherence in the aperiodic case, providing insights into the intricate relationship between temperature, hole distribution, and κ in SNMs.

Furthermore, the disparity $\eta_{\text{aperiodicity}}$ is more pronounced in SNMs with square holes than in those with circular holes. Once again, it is crucial to highlight the two potential mechanisms contributing to this divergence. Firstly, coherent phonons play

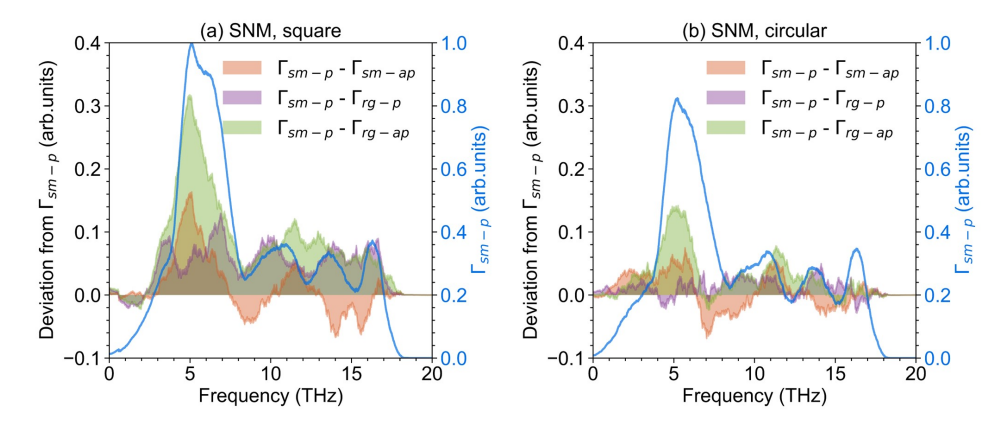


Figure 3: Left axis (shaded area): Deviation from phonon transmission spectra of SNMs with smooth periodically (Γ_{sm-p}) distributed holes; right axis (blue curve): phonon transmission spectra of Γ_{sm-p} . (a) SNMs with square holes (b) SNMs with circular holes.

a more substantial role in thermal transport within SNMs with square holes compared to those with circular holes, as the latter disrupt phonon coherence to a greater extent than the former. The substantial disruption of phonon coherence by uneven or rough surfaces/interfaces has been well-documented in prior studies. Secondly, circular holes exhibit strong phonon scattering, surpassing other phonon-blocking mechanisms, thus obscuring the influence of hole distribution on the overall κ .

A deeper understanding of the pronounced impact of hole boundary scattering on $\eta_{\text{aperiodicity}}$ emerges through a comparison of phonon transport in SNMs with smooth hole surfaces and those with rough hole surfaces. As depicted in Fig. 2, for SNMs with square holes, those featuring smooth surfaces exhibit a larger $\eta_{\text{aperiodicity}}$ than their counterparts with rough surfaces. This distinction arises from the fact that smooth hole surfaces scatter phonons less significantly, thereby better preserving phonon coherence. However, the impact of hole surface roughness on $\eta_{\text{aperiodicity}}$ in SNMs with circular holes is negligible. This is attributed to the circular holes functioning similarly to rough boundaries for phonons, regardless of whether the circular boundary is atomically smooth or rough.

3.1.3. Spectral transmission analysis To gain a more comprehensive understanding of the impact of hole boundary roughness, hole shape, and aperiodicity on phonon transport in SNMs, we conduct an in-depth analysis of the phonon transmission spectra for each SNM structure.

Figures 3a and 3b illustrate the phonon transmission spectra for SNMs with square holes and circular holes, respectively. In Fig. 3, the blue curve, plotted against the right axis, represents the phonon transmission spectra of SNMs with smooth and periodic (sm-p) holes. The shaded areas, plotted against the left axis, indicate the deviation of the phonon transmission spectra of smooth-aperiodic (sm-ap), rough-periodic (rg-p),

and rough-aperiodic (rg-ap) SNMs from the spectra of the smooth-periodic structure.

Specifically, the influence of hole distribution (periodic or aperiodic) on transmission spectra is quantified by the orange-colored area ($\Gamma_{\rm sm-p}$ - $\Gamma_{\rm sm-ap}$) in Fig. 3a. Evidently, aperiodicity markedly suppresses low-frequency (2-7 THz) phonon transport. This indeed agrees with the nature of coherent phonon transport in SL structures, where long-wavelength coherent phonons tend to be strongly suppressed (localized) by secondary aperiodicity. Interestingly, it even enhances phonon transmission in specific mid (7-10 THz) and high (13-16.5 THz) frequency regions.

In contrast, illustrated by the purple-colored area ($\Gamma_{\rm sm-p}$ - $\Gamma_{\rm rg-p}$) in Fig. 3a, hole boundary roughness markedly impedes phonon transmission across nearly the entire phonon spectrum. The substantial scattering of high-frequency phonons can be well explained by classical phonon scattering theory, where the surface specularity parameter is known to be positively correlated with the ratio of phonon wavelength to surface roughness. Higher-frequency acoustic phonons, having shorter wavelengths, exhibit lower specularity, implying a higher boundary scattering rate. The pronounced scattering of low-frequency phonons by hole boundary roughness may be attributed to the disrupted phonon coherence induced by surface irregularities. This phenomenon coincides with the frequency range where a substantial suppression of phonon transmission occurs due to aperiodic hole distribution, as depicted by the orange-colored region. Furthermore, prior research on SLs has indicated that interface roughness can markedly disrupt phonon coherence, diminishing the contribution of coherent phonons to thermal transport.

Moreover, the combined impact of aperiodicity and boundary roughness of holes on the phonon transmission spectra of SNM is elucidated by the green-colored area ($\Gamma_{\rm sm-p}$ - $\Gamma_{\rm rg-ap}$) in Fig. 3a. Notably, the green-colored area is approximately a linear combination of the orange one and the purple one, signifying that aperiodicity and boundary roughness can nearly independently suppress phonon transmission across the spectrum. This clarifies why rough-aperiodic SNMs exhibit significantly lower κ than their smooth-periodic counterparts. Consequently, rough-aperiodic SNMs emerge as promising candidates for low- κ materials, particularly in thermoelectric or thermal insulator applications. The distinctive combination of aperiodicity and hole boundary roughness significantly suppresses phonon transmission, leading to a notable reduction in κ . This reinforces their potential utility in applications where minimizing κ is crucial for optimal performance.

In the context of circular-hole SNMs, both commonalities and distinctions emerge when compared to square-hole SNMs. Firstly, as illustrated in Fig.3b, the orange-colored area indicates that aperiodically arranged holes still suppress lower-frequency phonons, albeit to a lesser extent, suggesting that circular holes inherently scatter phonons effectively. Moreover, the negligible presence of the purple-colored area in Fig.3b implies that surface roughness fails to exert a substantially additional impact on phonon suppression, contrasting with the scenario observed in square-holed SNMs depicted in Fig.3a. This observation aligns with the notion that circular holes function

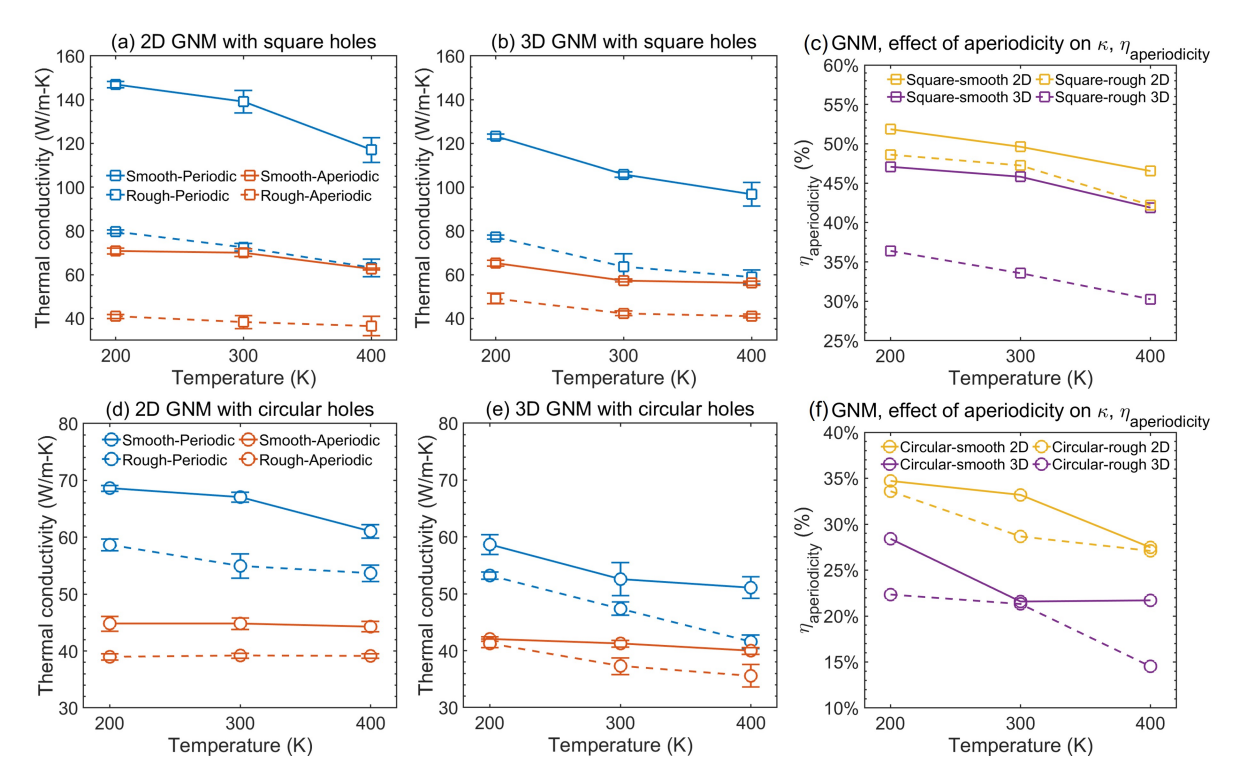


Figure 4: κ of GNMs at different temperatures. (a) 2D GNMs with square holes. (b) 3D GNMs with square holes. (c) The effectiveness of aperiodicity in reducing κ of GNMs with square holes. (d) 2D GNMs with circular holes. (e) 3D GNMs with circular holes. (f) The effectiveness of aperiodicity in reducing κ of GNMs with circular holes.

similarly to rough boundaries, resulting in an overlapping effect on phonon transport. Lastly, akin to the findings in square-hole SNMs, noticeable suppression of a broad spectrum of phonons occurs when the holes change from smooth and periodically arranged to rough and aperiodically arranged, as depicted by the green-colored area in Fig.3b. However, the magnitude of this suppression is less pronounced compared to that of square-hole SNMs in Fig. 3a.

In summary, our findings concerning SNMs suggest that circular (or, more generally, irregular) hole boundaries and hole surface roughness degrade phonon coherence and ballisticity in SNMs, diminishing the impact of randomizing hole locations on κ . This explains why phonon coherence was challenging to observe in previous experiments on SNMs, because the fabrication of nano-/micro-sized holes through focused-ion beam drilling or other methods inevitably resulted in substantial hole surface roughness. Additionally, several experiments utilized SNMs with circular holes, further exacerbating the challenge.

3.2. Graphene Nanomesh

3.2.1. Effect of dimensionality and hole shape, boundary roughness, and distribution on κ To gain deeper insights into the impact of hole morphology on phonon transport in

NM structures, our investigation will extend to GNMs. The singular atomic layer of GNMs results in an atomically thin hole boundary, akin to a 1D line structure. This characteristic provides a distinctive perspective for our analysis, allowing us to explore the intricate interplay between hole morphology and phonon behavior in nanomaterials.

It is noteworthy that in MD simulations, we have the convenience of selectively inhibiting atomic movements in one dimension (X, Y, or Z), enabling the realization of a purely 2D atomistic simulation. Utilizing this capability, we explore a conceptual, purely 2D GNM structure wherein atoms exclusively move in the in-plane directions. Such a modeled GNM exclusively exhibits in-plane phonons, omitting flexural phonons. This distinctive attribute introduces a dual impact on the overall κ of phonons. On one hand, it may diminish κ due to the absence of flexural phonon modes compared to a realistic 3D GNM, wherein atoms can move in all three dimensions. On the other hand, it may increase κ since in-plane phonons are not scattered by flexural phonons, unlike in a realistic 3D GNM.

Notably, our predictions indicate a κ of 1,073±72 W/m-K for 3D pristine graphene, in agreement with the original work that published the Tersoff potential parameters utilized in this study. In contrast, we predict a substantially higher κ of 2,490 ± 61 W/m-K for its 2D counterpart. This discrepancy suggests that the elimination of flexural phonons greatly reduces the scattering of in-plane phonons and thus increases their contribution to κ , outweighing the contribution of flexural phonons to κ in 3D graphene. Nonetheless, as evident from Fig. 4a and b, these two effects exhibit a similar influence on κ , nearly offsetting each other for the specific GNM structures investigated in this study, rendering only approximately 10% higher κ of 2D GNMs than their 3D counterparts.

Figure 4 elucidates the temperature-dependent characteristics of κ in GNMs, underscoring the heightened significance of anharmonic Umklapp scattering at the evaluated temperatures. The increased scattering rate, a well-known phenomenon in various crystalline or mildly defected materials, contributes to a reduction in κ . Additionally, a comparative analysis of κ between GNMs with square and circular holes, as depicted in Figs. 4a, b, d, and e, consistently demonstrates that GNMs with square holes exhibit higher κ than their circular-hole counterparts in both 2D and 3D configurations. Furthermore, GNMs with rough hole boundaries exhibit lower κ than their counterparts with smooth-hole boundaries.

3.2.2. The effectiveness of hole aperiodicity in reducing κ : comparison between SNM, 3D GNM, and conceptual 2D GNM. A prominent observation relevant to the focus of this work is the higher κ of GNMs with periodically arranged holes compared to their aperiodically arranged counterparts. Specifically, by directly examining the difference in κ between periodic and aperiodic GNMs, presented in Figs. 4c and 4f, we can deduce that: (1) GNMs with smooth hole boundaries display a larger $\eta_{\rm aperiodicity}$ than those with rough hole boundaries, (2) square-holed GNMs exhibit a larger $\eta_{\rm aperiodicity}$ than circular-holed ones, and (3) 2D GNMs manifest a larger $\eta_{\rm aperiodicity}$ than 3D GNMs. Furthermore,

the $\eta_{\rm aperiodicity}$ of all the GNM structures decreases significantly with rising temperature, which is featured by increased anharmonic phonon-phonon scattering. Therefore, we can conclude that structures with less phonon scattering, whether intrinsic or extrinsic, exhibit a larger $\eta_{\rm aperiodicity}$. These insights, derived from GNMs, align with and reinforce our findings in SNMs, underscoring their shared characteristics. It is worth noting that we do not reiterate the discussion of the underlying mechanisms for the aforementioned observations; readers are directed to the previous section for this detailed information.

Therefore, to observe a significant impact of aperiodicity on κ of NMs in experiments, it is imperative to maintain high crystallinity and purity in the NM structure, ensure the smoothness of hole boundaries, and conduct measurements at low temperatures. This elucidates why prior experiments, showcasing distinct phonon coherence, were conducted at a few Kelvins. Nevertheless, it is essential to acknowledge the considerable challenge in achieving these conditions with modern techniques capable of drilling holes in thin films or 2D materials, such as focused-ion beam techniques.

3.2.3. Spectral phonon transmission analysis Figure. 5 shows the phonon transmission spectra of 2D GNMs and 3D GNMs, with the latter decomposed into in-plane phonon and flexural phonon contributions.

Illustrated by the orange-colored areas $(\Gamma_{sm-p} - \Gamma_{sm-ap})$ in Fig. 5a and Fig. 5b, aperiodic hole distribution significantly inhibits in-plane phonons in GNMs with smooth-boundary square holes, particularly in the mid-to-high frequency range. This frequency range corresponds to the spectrum of the longitudinal acoustic phonon branch of pristine graphene. While the introduction of holes into the graphene layer modifies the dispersion relations, we assert that, on the whole, the frequency of longitudinal acoustic phonons remains largely unchanged.

The purple-colored areas $(\Gamma_{sm-p} - \Gamma_{rg-p})$ in both Fig.5a and Fig.5b illustrate the impact of hole boundary roughness on in-plane phonon transmission spectra. Clearly, roughness inhibits a broad spectrum of in-plane phonons, encompassing both acoustic and optical phonon modes in graphene.

On the other hand, as depicted in Fig. 5c, both aperiodicity and roughness contribute to the suppression of the entire spectrum of flexural phonons, spanning both acoustic and optical ranges. However, it is noteworthy that roughness induces significantly stronger suppression compared to aperiodicity. Once again, we emphasize that, akin to the cases of SNMs and SLs, boundary roughness has the capacity to reduce the κ of structures with secondary periodicity through both phonon-boundary scattering and phonon decoherence, while aperiodicity only leads to the latter.

Figures 5d-f present the transmission spectra of GNMs with circular holes. Evidently, neither aperiodicity (indicated by the orange-colored areas) nor hole boundary roughness (indicated by the purple-colored areas) causes a substantial suppression of phonon transmission compared to the scenarios observed in square-holed GNMs. This is attributed to the inherent nature of circular holes, which inherently function as robust rough boundaries, significantly scattering phonons across a wide

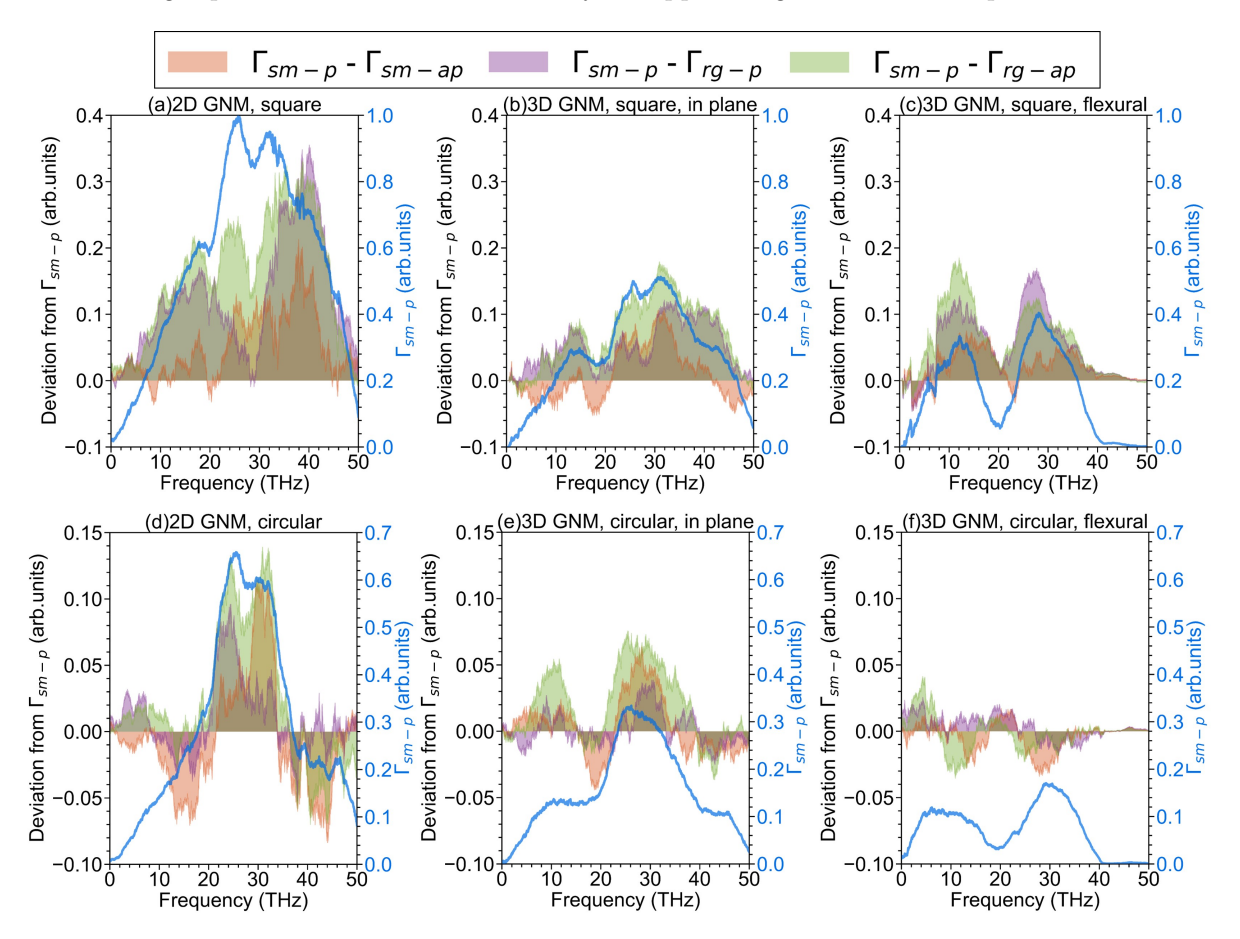


Figure 5: Left axis (shaded area): Deviation from phonon transmission spectra Γ_{sm-p} ; right axis (blue curve): phonon transmission spectra of Γ_{sm-p} . (a) 2D GNMs with square holes (b) in-plane phonons in 3D GNMs with square holes (c) flexural phonons in 3D GNMs with square holes (d) 2D GNMs with circular holes (e) in-plane phonons in 3D GNMs with circular holes.

spectrum. The influence of aperiodicity and hole boundary roughness on flexural phonon transmission is nearly negligible in circular-holed SNMs. This is due to the strong scattering of flexural phonons by boundary roughness, as previously demonstrated in Fig. 5c. Consequently, their contribution is already diminished by the circular boundaries before roughness comes into play.

3.2.4. A comparison between $\eta_{aperiodicity}$ of SNM, 3D GNM, and conceptual 2D GNM Given the distinctive features of GNMs with a 1D-line-like hole boundary and SNMs with a 2D surface-like hole boundary, as illustrated in Fig. 6, a comparison of the results for these two NM structures is essential. Upon careful examination of Fig.2c and Fig.4c, a discernible trend emerges. While $\eta_{aperiodicity}$ exhibits a similarity in SNMs and GNMs with smooth-boundary-square holes, a noteworthy disparity becomes evident in the two structures when the hole boundaries are rough. Specifically, $\eta_{aperiodicity}$ of rough-holed SNMs is significantly higher than that of GNMs. This discrepancy is likely

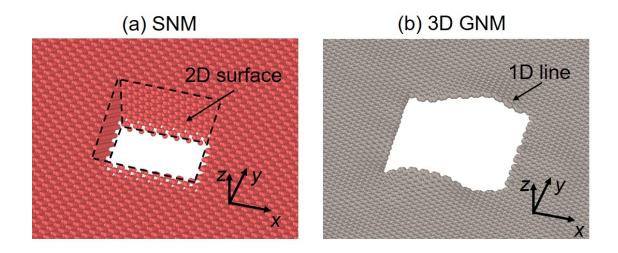


Figure 6: Illustrations of 1D line-like and 2D surface-like hole boundaries. (a) 2D surface-like hole boundary in SNM. (b) 1D line-like hole boundary in 3D GNM.

attributed to the more pronounced hole boundary scattering of phonons (relative to intrinsic scattering mechanisms) in GNMs compared to SNMs. This observation aligns with the understanding that the dangling edges in graphene can markedly scatter or localize phonons[39, 40], consequently reducing κ , as observed in previous studies on graphene nanoribbons or other nano-graphene structures. In contrast, the 2D surface-like hole boundaries in SNMs are more mechanically stable than the 1D line-like hole edges in GNMs, resulting in less scattering or trapping of phonons. These observations indicate that SNMs, or more generally, 3D material thin films with extended through holes, constitute a more robust system than 2D material NMs like GNMs, showcasing a significant $\eta_{\rm aperiodicity}$ even in the presence of hole boundary roughness.

4. Conclusion

In this study, we conducted an extensive investigation into phonon thermal transport across NMs with diverse structural characteristics. Our key finding is that NMs, whether composed of 2D or 3D materials, with smooth and planar hole boundaries, serve as optimal systems to showcase the effect of aperiodicity in hole distribution on reducing κ . Additionally, our rigorous analysis of phonon transmission spectra revealed that aperiodic hole distribution predominantly suppresses acoustic phonon transport, particularly low-frequency acoustic phonons in SNMs, while roughness impedes the transport of a broad range of phonons, encompassing both acoustic and optical phonons.

It is noteworthy that hole boundary roughness is inevitable in current experimental techniques for NM fabrication. As a result, SNMs, or more generally, NM films made of 3D materials, emerge as more robust systems than GNM or other 2D material NMs for demonstrating significant $\eta_{\rm aperiodicity}$. Our work provides valuable guidance for designing optimal NM structures to showcase phonon coherence behaviors, facilitating the application of this intriguing structure type in thermoelectric materials or other applications.

Finally, it is worth noting that recent advancements have facilitated the scalable manufacturing of GNMs [41–43], offering promising prospects for applications requiring ultralow κ . These GNMs, characterized by aperiodically distributed, non-square holes with certain hole boundary roughness, hold potential for various applications,

Elucidating Optimal Nanohole Structures for Suppressing Phonon Transport in Nanomeshes15

including thermoelectric devices. However, achieving optimal performance in such applications necessitates a systematic approach to optimize the electron properties, including electrical conductivity and Seebeck coefficient, to exploit the potential of GNMs fully.

Acknowledgements

H. Cui and Y. Wang gratefully acknowledge the support provided by the National Science Foundation (Award No. 2047109). T. Ma received support from the National Science Foundation (Award No. 1826392). The authors thank the support of Research & Innovation and the Office of Information Technology at the University of Nevada, Reno for facilitation and access to the Pronghorn High-Performance Computing Cluster.

References

[1] Jingwei Bai, Xing Zhong, Shan Jiang, Yu Huang, and Xiangfeng Duan. Graphene nanomesh. *Nature Nanotechnology*, 5(3):190–194, Mar 2010. ISSN 1748-3395. doi: 10.1038/nnano.2010.8. URL https://doi.org/10.1038/nnano.2010.8.

- [2] Jen-Kan Yu, Slobodan Mitrovic, Douglas Tham, Joseph Varghese, and James R. Heath. Reduction of thermal conductivity in phononic nanomesh structures. Nature Nanotechnology, 5(10):718–721, Oct 2010. ISSN 1748-3395. doi: 10.1038/nnano.2010.149. URL https://doi.org/10.1038/nnano.2010.149.
- [3] Jinyao Tang, Hung-Ta Wang, Dong Hyun Lee, Melissa Fardy, Ziyang Huo, Thomas P. Russell, and Peidong Yang. Holey silicon as an efficient thermoelectric material. *Nano Letters*, 10(10):4279–4283, Oct 2010. ISSN 1530-6984. doi: 10.1021/nl102931z. URL https://doi.org/10.1021/nl102931z.
- [4] Patrick E. Hopkins, Charles M. Reinke, Mehmet F. Su, Roy H. Olsson III, Eric A. Shaner, Zayd C. Leseman, Justin R. Serrano, Leslie M. Phinney, and Ihab El-Kady. Reduction in the thermal conductivity of single crystalline silicon by phononic crystal patterning. *Nano Letters*, 11(1):107–112, Jan 2011. ISSN 1530-6984. doi: 10.1021/nl102918q. URL https://doi.org/10.1021/nl102918q.
- [5] Seyedhamidreza Alaie, Drew F. Goettler, Mehmet Su, Zayd C. Leseman, Charles M. Reinke, and Ihab El-Kady. Thermal transport in phononic crystals and the observation of coherent phonon scattering at room temperature. *Nature Communications*, 6(1):7228, Jun 2015. ISSN 2041-1723. doi: 10.1038/ncomms8228. URL https://doi.org/10.1038/ncomms8228.
- [6] Pranay Chakraborty, Tengfei Ma, Amir Hassan Zahiri, Lei Cao, Yan Wang, et al. Carbon-based materials for thermoelectrics. Advances in Condensed Matter Physics, 2018, 2018.
- [7] Qing Hao, Gang Chen, and Ming-Shan Jeng. Frequency-dependent Monte Carlo simulations of phonon transport in two-dimensional porous silicon with aligned pores. *Journal of Applied Physics*, 106(11):114321, 12 2009. ISSN 0021-8979. doi: 10.1063/1.3266169. URL https://doi.org/10.1063/1.3266169.
- [8] Ankit Jain, Ying-Ju Yu, and Alan J. H. McGaughey. Phonon transport in periodic silicon nanoporous films with feature sizes greater than 100 nm. *Phys. Rev. B*, 87:195301, May 2013. doi: 10.1103/PhysRevB.87.195301. URL https://link.aps.org/doi/10.1103/PhysRevB.87.195301.
- [9] Maria N. Luckyanova, Jivtesh Garg, Keivan Esfarjani, Adam Jandl, Bulsara, J. Schmidt, Mayank Τ. Aaron Austin J. Minnich, Shuo Chen. Mildred S. Dresselhaus, Zhifeng Ren, Eugene A. Fitzgerald, and Gang Chen. Coherent phonon heat conduction in superlattices. Sci-338(6109):936–939, 10.1126/science.1225549. 2012. doi: URL ence, https://www.science.org/doi/abs/10.1126/science.1225549.

[10] Yan Wang, Haoxiang Huang, and Xiulin Ruan. Decomposition of coherent and incoherent phonon conduction in superlattices and random multilayers. *Phys. Rev. B*, 90:165406, Oct 2014. doi: 10.1103/PhysRevB.90.165406. URL https://link.aps.org/doi/10.1103/PhysRevB.90.165406.

- [11] Jayakanth Ravichandran, Ajay K. Yadav, Ramez Cheaito, Pim B. Rossen, Arsen Soukiassian, S. J. Suresha, John C. Duda, Brian M. Foley, Che-Hui Lee, Ye Zhu, Arthur W. Lichtenberger, Joel E. Moore, David A. Muller, Darrell G. Schlom, Patrick E. Hopkins, Arun Majumdar, Ramamoorthy Ramesh, and Mark A. Zurbuchen. Crossover from incoherent to coherent phonon scattering in epitaxial oxide superlattices. *Nature Materials*, 13(2):168–172, Feb 2014. ISSN 1476-4660. doi: 10.1038/nmat3826. URL https://doi.org/10.1038/nmat3826.
- [12] Pranay Chakraborty, Lei Cao, and Yan Wang. Ultralow lattice thermal conductivity of the random multilayer structure with lattice imperfections. *Scientific Reports*, 7(1):8134, Aug 2017. ISSN 2045-2322. doi: 10.1038/s41598-017-08359-2. URL https://doi.org/10.1038/s41598-017-08359-2.
- [13] M. N. Luckyanova, J. Mendoza, H. Lu, B. Song, S. Huang, J. Zhou, M. Li, Y. Dong, H. Zhou, J. Garlow, L. Wu, B. J. Kirby, A. J. Grutter, A. A. Puretzky, Y. Zhu, M. S. Dresselhaus, A. Gossard, and G. Chen. Phonon localization in heat conduction. *Science Advances*, 4(12):eaat9460, 2018. doi: 10.1126/sciadv.aat9460. URL https://www.science.org/doi/abs/10.1126/sciadv.aat9460.
- [14] Run Hu, Sotaro Iwamoto, Lei Feng, Shenghong Ju, Shiqian Hu, Masato Ohnishi, Naomi Nagai, Kazuhiko Hirakawa, and Junichiro Shiomi. Machine-learning-optimized aperiodic superlattice minimizes coherent phonon heat conduction. *Phys. Rev. X*, 10:021050, Jun 2020. doi: 10.1103/PhysRevX.10.021050. URL https://link.aps.org/doi/10.1103/PhysRevX.10.021050.
- [15] Tengfei Ma, Cheng-Te Lin, and Yan Wang. The dimensionality effect on phonon localization in graphene/hexagonal boron nitride superlattices. 2D Materials, 7(3):035029, jun 2020. doi: 10.1088/2053-1583/ab93e2. URL https://dx.doi.org/10.1088/2053-1583/ab93e2.
- [16] Pranay Chakraborty, Yida Liu, Tengfei Ma, Xixi Guo, Lei Cao, Run Hu, and Yan Wang. Quenching thermal transport in aperiodic superlattices: A molecular dynamics and machine learning study. ACS Applied Materials & Interfaces, 12(7):8795–8804, 2020. doi: 10.1021/acsami.9b18084. URL https://doi.org/10.1021/acsami.9b18084. PMID: 31994867.
- [17] Jaeho Lee, Woochul Lee, Geoff Wehmeyer, Scott Dhuey, Deirdre L. Olynick, Stefano Cabrini, Chris Dames, Jeffrey J. Urban, and Peidong Yang. Investigation of phonon coherence and backscattering using silicon nanomeshes. *Nature Communications*, 8:1–8, 2017. ISSN 20411723. doi: 10.1038/ncomms14054.
- [18] Gang Chen Bo Qiu and Zhiting Tian. Effects of aperiodicity and roughness on coherent heat conduction in superlattices. *Nanoscale and Microscale Thermophys*-

ical Engineering, 19(4):272-278, 2015. doi: 10.1080/15567265.2015.1102186. URL https://doi.org/10.1080/15567265.2015.1102186.

- [19] Yan Wang, Chongjie Gu, and Xiulin Ruan. Optimization of the random multilayer structure to break the random-alloy limit of thermal conductivity. *Applied Physics Letters*, 106(7):073104, 02 2015. ISSN 0003-6951. doi: 10.1063/1.4913319. URL https://doi.org/10.1063/1.4913319.
- [20] Pranay Chakraborty, Isaac Armstrong Chiu, Tengfei Ma, and Yan Wang. Complex temperature dependence of coherent and incoherent lattice thermal transport in superlattices. *Nanotechnology*, 32(6):065401, nov 2020. doi: 10.1088/1361-6528/abc2ef. URL https://dx.doi.org/10.1088/1361-6528/abc2ef.
- [21] Tianli Feng and Xiulin Ruan. Ultra-low thermal conductivity in nanomesh. Carbon, 101:107-113, 2016. **ISSN** 0008graphene 6223. doi: https://doi.org/10.1016/j.carbon.2016.01.082. URL https://www.sciencedirect.com/science/article/pii/S0008622316300707.
- [22] Han Wei, Yue Hu, Hua Bao, and Xiulin Ruan. Quantifying the diverse wave effects in thermal transport of nanoporous graphene. *Carbon*, 197:18–26, 2022. ISSN 0008-6223. doi: https://doi.org/10.1016/j.carbon.2022.06.011. URL https://www.sciencedirect.com/science/article/pii/S0008622322004419.
- [23] Yan Wang, Ajit K Vallabhaneni, Bo Qiu, and Xiulin Ruan. Two-dimensional thermal transport in graphene: a review of numerical modeling studies. *Nanoscale and Microscale Thermophysical Engineering*, 18(2):155–182, 2014.
- [24] Aidan P. Thompson, H. Metin Aktulga, Richard Berger, Dan S. Bolintineanu, W. Michael Brown, Paul S. Crozier, Pieter J. in 't Veld, Axel Kohlmeyer, Stan G. Moore, Trung Dac Nguyen, Ray Shan, Mark J. Stevens, Julien Tranchida, Christian Trott, and Steven J. Plimpton. Lammps a flexible simulation tool for particle-based materials modeling at the atomic, meso, and continuum scales. *Computer Physics Communications*, 271:108171, 2022. ISSN 0010-4655. doi: https://doi.org/10.1016/j.cpc.2021.108171. URL https://www.sciencedirect.com/science/article/pii/S0010465521002836.
- Weber. [25] Frank H. Stillinger and Thomas Α. Computer simulaorder in condensed phases of silicon. Phys. Rev. B.tion of local 31:5262-5271, Apr 1985. doi: 10.1103/PhysRevB.31.5262. URL https://link.aps.org/doi/10.1103/PhysRevB.31.5262.
- [26] Cem Sevik, Alper Kinaci, Justin B. Haskins, and Tahir Çağ ın. Characterization of thermal transport in low-dimensional boron nitride nanostructures. *Phys. Rev. B*, 84:085409, Aug 2011. doi: 10.1103/PhysRevB.84.085409. URL https://link.aps.org/doi/10.1103/PhysRevB.84.085409.
- [27] Kimmo Sääskilahti, Jani Oksanen, Jukka Tulkki, and Sebastian Volz. Role of anharmonic phonon scattering in the spectrally decomposed thermal conductance at planar interfaces. *Physical Review B*, 90(13):134312, 2014.

[28] Kimmo Sääskilahti, Jani Oksanen, Sebastian Volz, and Jukka Tulkki. Frequency-dependent phonon mean free path in carbon nanotubes from nonequilibrium molecular dynamics. *Physical Review B*, 91(11):115426, 2015.

- [29] Yan Wang, Bo Qiu, and Xiulin Ruan. Edge effect on thermal transport in graphene nanoribbons: A phonon localization mechanism beyond edge roughness scattering. *Applied Physics Letters*, 101(1), 2012.
- [30] Bo Qiu, Yan Wang, Qing Zhao, and Xiulin Ruan. The effects of diameter and chirality in the thermal transport in free-standing and supported carbon-nanotubes. In *International Conference on Micro/Nanoscale Heat Transfer*, volume 54778, pages 633–638. American Society of Mechanical Engineers, 2012.
- Yarifard, J. Davoodi, and Η. Rafii-Tabar. In-plane thermal graphene nanomesh: dynamics conductivity of Α molecular study. Computational MaterialsScience,111:247-251, 2016. ISSN 0927-0256.doi: https://doi.org/10.1016/j.commatsci.2015.09.033. URL https://www.sciencedirect.com/science/article/pii/S0927025615006023.
- [32] Theodore Maranets and Yan Wang. Ballistic phonon lensing by the non-planar interfaces of embedded nanoparticles. New Journal of Physics, 25(10):103038, oct 2023. doi: 10.1088/1367-2630/ad025a. URL https://dx.doi.org/10.1088/1367-2630/ad025a.
- [33] Theodore Maranets, Milad Nasiri, and Yan Wang. Influence of spatial coherence on phonon transmission across aperiodically arranged interfaces. arXiv preprint arXiv:2403.01321, 2024.
- [34] Jinwoo Oh, Hoyeon Yoo, Jaeyoo Choi, Jeong Yun Kim, Dong Su Lee, Myung Jong Kim, Jong-Chan Lee, Woo Nyon Kim, Jeffrey C. Grossman, Jong Hyuk Park, Sang-Soo Lee, Heesuk Kim, and Jeong Gon Son. Significantly reduced thermal conductivity and enhanced thermoelectric properties of single- and bilayer graphene nanomeshes with sub-10nm neck-width. *Nano Energy*, 35:26–35, 2017. ISSN 2211-2855. doi: https://doi.org/10.1016/j.nanoen.2017.03.019. URL https://www.sciencedirect.com/science/article/pii/S2211285517301507.
- [35] Shiqian Hu, Zhongwei Zhang, Pengfei Jiang, Jie Chen, Sebastian Volz, Masahiro Nomura, and Baowen Li. Randomness-induced phonon localization in graphene heat conduction. *The Journal of Physical Chemistry Letters*, 9(14):3959–3968, 2018. doi: 10.1021/acs.jpclett.8b01653. URL https://doi.org/10.1021/acs.jpclett.8b01653. PMID: 29968477.
- [36] Sabry G Moustafa, Andrew J Schultz, and David A Kofke. Very fast averaging of thermal properties of crystals by molecular simulation. *Physical Review E*, 92(4): 043303, 2015.
- [37] Shigeo Maruyama. A molecular dynamics simulation of heat conduction of a finite length single-walled carbon nanotube. *Microscale Thermophysical Engineering*, 7 (1):41–50, 2003.

[38] John A Thomas, Joseph E Turney, Ryan M Iutzi, Cristina H Amon, and Alan JH McGaughey. Predicting phonon dispersion relations and lifetimes from the spectral energy density. *Physical Review B*, 81(8):081411, 2010.

- [39] Yan Wang, Bo Qiu, and Xiulin Ruan. Edge effect on thermal transport in graphene nanoribbons: A phonon localization mechanism beyond edge roughness scattering. *Applied Physics Letters*, 101(1):013101, 07 2012. ISSN 0003-6951. doi: 10.1063/1.4732155. URL https://doi.org/10.1063/1.4732155.
- [40] Yan Wang, Ajit Vallabhaneni, Jiuning Hu, Bo Qiu, Yong P. Chen, and Xiulin Ruan. Phonon lateral confinement enables thermal rectification in asymmetric single-material nanostructures. *Nano Letters*, 14(2):592–596, 2014. doi: 10.1021/nl403773f. URL https://doi.org/10.1021/nl403773f. PMID: 24393070.
- [41] Dini Wang, Rui Dai, Xing Zhang, Lei Liu, Houlong Zhuang, Yongfeng Lu, Yan Wang, Yiliang Liao, and Qiong Nian. Scalable and controlled creation of nanoholes in graphene by microwave-assisted chemical etching for improved electrochemical properties. *Carbon*, 161:880–891, 2020.
- [42] Kun Bi, Dini Wang, Rui Dai, Lei Liu, Yan Wang, Yongfeng Lu, Yiliang Liao, Ling Ding, Houlong Zhuang, and Qiong Nian. Scalable nanomanufacturing of holey graphene via chemical etching: an investigation into process mechanisms. *Nanoscale*, 14(12):4762–4769, 2022.
- [43] Dini Wang, Yan Dou, Xing Zhang, Kun Bi, Iyyappa Rajan Panneerselvam, Haofan Sun, Xinyu Jiang, Rui Dai, Kenan Song, Houlong Zhuang, Yongfeng Lu, Yan Wang, Yiliang Liao, Ling Ding, and Qiong Nian. Manufacturing and applications of multifunctional holey two-dimensional nanomaterials a review. *Nano Today*, 55:102162, 2024. ISSN 1748-0132. doi: https://doi.org/10.1016/j.nantod.2024.102162. URL https://www.sciencedirect.com/science/article/pii/S1748013224000173.